36

INDUCTIVE THEORY OF SHEAR FLOWS

GIANNI JARRE
Politecnico di Torino, Italy

In the boundary layer past an airfoil four characteristic points follow one another (Fig. 1):

I the stagnation point at the leading edge
II the point of maximum wall shear-stress
III the point of maximum outer velocity
IV the separation point

Any approximate method for describing the laminar boundary layer past airfoils must also describe, as a particular case, the similar laminar flows past wedges. These last flows fulfill the well known equation of Falkner and Skan[1]

$$f''' + ff'' + \frac{2m}{m+1}(1 - f'^2) = 0 \qquad (1)$$

where $u/U = \varphi = f'$, with $f(0) = f'(0) = 0$ and $f'(\infty) = 1$; $m = xdU/Udx$ is the only parameter of the outer velocity law $U \sim x^m$.

In the set of such exact profiles the four characteristic points are labeled by the following values of exponent m: 1, 1/3, 0, − 0.091, respectively.

In the upper part of Fig. 2 these four exact profiles are drawn according to the numberical solution of Eq. (1) given by Hartree.[2] The ordinate is the normalized velocity $\varphi = u/U$ and the abscissa is by convention = 0 for $\varphi = 0$ and = 1 for $\varphi = \frac{1}{2}$. In the lower part of Fig. 2 the corresponding four shear-stress profiles are drawn as obtained by mere numerical derivation from velocity profiles.

SYMBOLS

f = Normalized stream function
F = Auxiliary function
K = Third shape factor
m = Falkner & Skan's parameter
t = Normalized shear-stress
u = Velocity along x-axis

U = Outer velocity
v = Velocity along y-axis
x = Abscissa
y = Ordinate
α, β, γ = Linear multiplicators, Eqs. (20), (21), and (22)
δ = Boundary layer thickness
δ^* = Displacement thickness
ϵ = Eddy viscosity
θ = Momentum thickness
η = Normalized ordinate
λ = Linear multiplicator, Eq. (19)
Λ = Pohlhausen's parameter
μ = Dynamic viscosity
τ = Shear-stress
φ = Normalized velocity

Only for profiles I, II, III the ordinate is the normalized shear-stress $t = \tau/\tau_0$ and again the abscissa is by convention = 0 for $t = 1$ and = 1 for $t = \frac{1}{2}$; as for profile IV of separation, having $\tau_0 = 0$, it is enough to say that the ordinate is proportional to the shear-stress.

Since the equally hachured diagrams of Fig. 2 are actually almost equal, the following empirical rule arises:

- each velocity profile is complementary to the preceding shear-stress profile.

Otherwise, aside from normalization:

- each velocity profile has the shape of the derived preceding one.

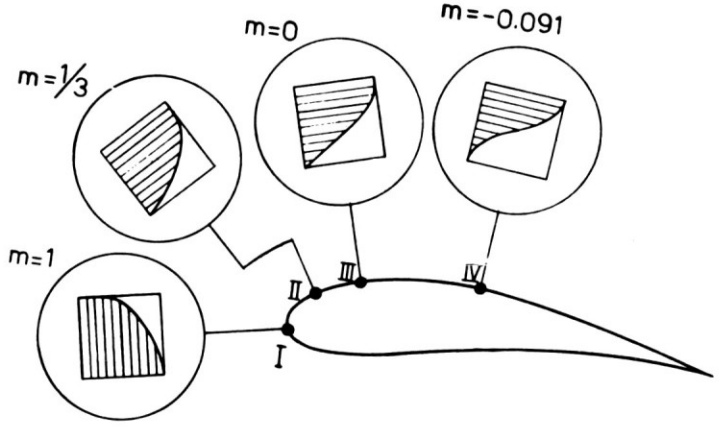

Fig. 1. Qualitative picture of the laminar velocity profiles at the four characteristic points on an airfoil: I, stagnation point; II, τ_0-max point; III, U-max point; IV, separation point.

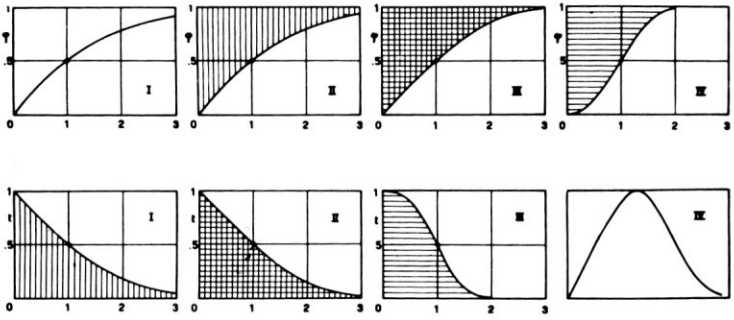

Fig. 2. Laminar normalized velocity profiles and shear-stress profiles at the four characteristic points on an airfoil: I, stagnation point; II, τ_0-max point; III, U-max point; IV, separation point.

Such *rule of progressive derivatives* is stated by the following set of equations:

$$\begin{cases} \varphi_{II} + t_I = 1 \\ \varphi_{III} + t_{II} = 1 \\ \varphi_{IV} + t_{III} + 1 \end{cases} \tag{2}$$

bound to one another because each t is the normalized derivative of the corresponding φ.

Let us now accept the assumption, also implied in Pohlhausen method,[1] that the velocity profiles in the boundary layer past an airfoil are shaped exactly as in the corresponding tangent wedges.

Then the laminar boundary layer behaves like a computer which progressively derives the stagnation profile; hence the velocity profiles are progressively simplified when passing from the leading edge to the separation point.

Therefore we will start from the simplest profile, i.e., from the shear-stress profile of separation; thereafter the rule (2), by progressive normalized integrations, will give all the velocity profiles up to the stagnation point.

Let us define now $\eta = y/\delta$, where δ is the boundary layer thickness; of course in laminar régime t and φ are bound as follows:

$$\varphi = \int_0^\eta t d\eta \Big/ \int_0^1 t d\eta \tag{3}$$

Let us define, besides, for the separation point, where $\tau_0 = 0$ but $\tau y_0 \neq 0$.

$$t_{IV} = \tau/\delta\tau_{y0} \qquad \text{i.e., } t_{IV} \to \eta \quad \text{as} \quad \eta \to 0 \tag{4}$$

Since the separation profile behaves like a half-wake, an even function for $\varphi_{IV}(\eta)$ or an odd function for $t_{IV}(\eta)$ may be reasonably assumed. Thus the family of functions $t_{IV} = \eta(1 - \eta^2)^i$ was tested in the field $0 \leq i \leq 5$; $i = 1$ resulted as the best exponent for describing the separation.

When t_{IV} is so chosen:

$$t_{IV} = \eta(1 - \eta^2) \tag{5}$$

from Eq. (3) the *separation profile* is obtained:

$$\varphi_{IV} = 1 - (1 - \eta)^2(1 + 2\eta + \eta^2) = 2\eta^2 - \eta^4 \tag{6}$$

Then the third of rules (2) gives:

$$t_{III} = (1 - \eta)^2(1 + 2\eta + \eta^2) = (1 - \eta^2)^2 \tag{7}$$

and from Eq. (3) the *maximum velocity profile* is obtained:

$$\varphi_{III} = 1 - (1 - \eta)^3(1 + 9\eta/8 + 3\eta^2/8) = (15\eta - 10\eta^3 + 3\eta^5)/8 \tag{8}$$

Then the second of rules (2) gives:

$$t_{II} = (1 - \eta)^3(1 + 9\eta/8 + 3\eta^2/8) \tag{9}$$

and from Eq. (3) the *maximum shear-stress profile* is obtained:

$$\varphi_{II} = 1 - (1 - \eta)^4(1 + 4\eta/5 + \eta^2/5) = (16\eta - 15\eta^2 + 5\eta^4 - \eta^6)/5 \tag{10}$$

Then the first of rules (2) gives:

$$t_I = (1 - \eta)^4(1 + 4\eta/5 + \eta^2/5) \tag{11}$$

and from Eq. (3) the *stagnation profile* is obtained:

$$\varphi_I = 1 - (1 - \eta)^5(1 + 5\eta/8 + \eta^2/8) \tag{12}$$

$$= (35\eta - 56\eta^2 + 35\eta^3 - 7\eta^5 + \eta^7)/8$$

At the outer edge ($\eta = 1$) the velocity defect ($1 = \varphi$) vanishes with decreasing zeros from the 5th to the 2nd order, when passing from the stagnation to the separation point.

On the contrary in the well known set of Pohlhausen profiles:

$$t = (1 - \eta)^2\left[1 + 4\eta\,\frac{6 - \Lambda}{12 + \Lambda}\right] \tag{13}$$

$$\varphi = 1 - (1 - \eta)^3\left[1 + \eta\,\frac{6 - \Lambda}{6}\right] \tag{14}$$

the velocity defect ($1 - \varphi$) always has an outer zero of 3rd order.

According to Pohlhausen:

- Eq. (14) with $\Lambda = -12$ describes the separation profile (IV):

$$\varphi = 1 - (1 - \eta)^3(1 + 3\eta) = 6\eta^2 - 8\eta^3 + 3\eta^4 \tag{15}$$

- Eq. (14) with $\Lambda = 0$ describes the maximum velocity profile (III):

$$\varphi = 1 - (1 - \eta)^3(1 + \eta) = 2\eta - 2\eta^3 + \eta^4 \tag{16}$$

- the maximum shear-stress profile is not recognizable in Eq. (14),
- Eq. (14) with $\Lambda = 7.052$ describes the stagnation profile (I):

$$\varphi = 1 - (1 - \eta)^3(1 - 0.1753\eta) \tag{17}$$

We are able now to calculate the following classical shape-factors:

$$\left.\begin{aligned} \delta^*/\theta &= \int_0^1 (1 - \varphi)\, d\eta \Big/ \int_0^1 \varphi\,(1 - \varphi)\, d\eta \\ \tau_0\theta/\mu u &= \varphi_0' \int_0^1 \varphi\,(1 - \varphi)\, d\eta \\ K &= -\varphi_0'' \left[\int_0^1 \varphi\,(1 - \varphi)\, d\eta\right]^2 \\ F &= 2\left[\frac{\tau_0\theta}{\mu u} - K\left(2 + \frac{\delta^*}{\theta}\right)\right] \end{aligned}\right\} \tag{18}$$

The numerical results are reported in Table I.

As for the stagnation point, profile (17) succeeds in giving exactly $F = 0$ because the special value $\Lambda = 7.052$ was chosen ad hoc; whilst profile (12), lacking available parameters, gives $F = -0.073$, i.e., thicknesses δ, δ^*, θ, slightly decreasing versus x at the leading edge. Except for this, the set of profiles (6, 8, 10, 12) comes closer to exact results than the set (15, 16, 17) does, and in particular:

- for the maximum velocity point, profile (8) is even better than the already good profile (16), as Table I shows and Fig. 3 directly confirms,
- for the separation point, profile (6) is a strong improvement over profile (15), as Table I shows and Fig. 4 directly confirms.

TABLE I

Point	I: Stagnation Point			II: τ_0-Max. Point			III: U-Max. Point			IV: Separation Point		
Eq.	(1)	(12)	(17)	(1)	(10)	—	(1)	(8)	(16)	(1)	(6)	(15)
δ^*/θ	2.227	2.247	2.308	2.309	2.346	—	2.605	2.596	2.554	4.034	4.200	3.500
$\tau_0\theta/\mu U$	0.360	0.355	0.332	0.323	0.312	—	0.220	0.226	0.235	0.000	0.000	0.000
1,000 K	85.3	92.0	77.0	60.5	57.0	—	0.000	0.000	0.000	−68.0	−64.5	−156.7
1,000 F	0	−73	0	124	129	—	440	452	470	820	800	1,724

In order to describe all the nuances of pressure gradient, Pohlhausen used the linear combination (14) of the two profiles (15), (16), namely:

$$\varphi = (1 - \lambda)\varphi_{16} + \lambda\varphi_{15} \qquad \text{with} \qquad \lambda = -\Lambda/12 \tag{19}$$

$\lambda = 0$ and $\lambda = 1$ again describe maximum velocity and separation profiles; $\lambda < 0$ and $\lambda > 0$ describe accelerated and retarded flows.

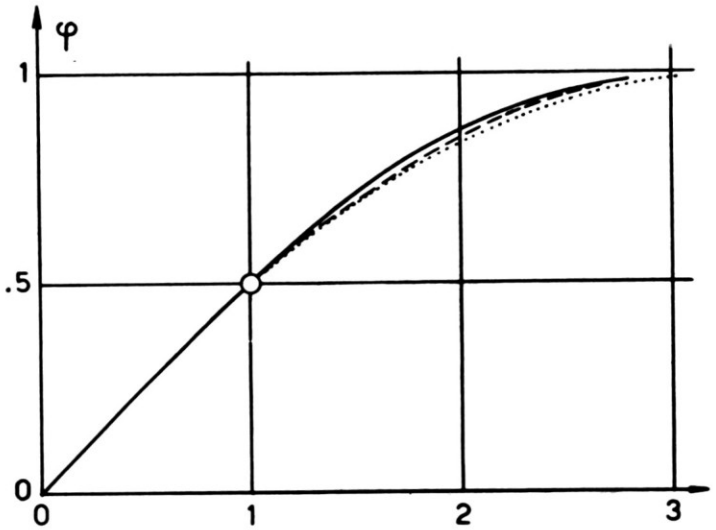

Fig. 3. Laminar velocity profiles at the maximum velocity point, according to: . . . . . Pohlhausen method, Eq. (16); - - - present method, Eq. (8); —— exact Blasius solution, Eq. (1) with $m = 0$ (abscissa = 1 for $\varphi = 0.5$).

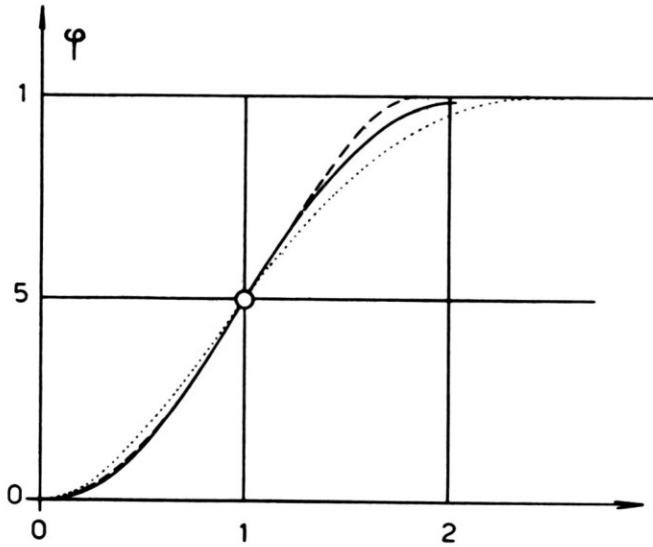

Fig. 4. Laminar velocity profiles at the separation point, according to: . . . . . Pohlhausen method, Eq. (15); - - - present method, Eq. (6); —— exact Hartree solution, Eq. (1) with $m = 0.091$ (abscissa = 1 for $\varphi = 0.5$).

On the contrary the rule of progressive derivatives requires different treatments for each range of pressure gradient. Following the model of Eq. (19) we may describe, but in three steps, all the nuances of pressure gradient:

$$\varphi = (1 - \alpha)\varphi_{\mathrm{I}} + \alpha\varphi_{\mathrm{II}} \qquad 0 \leq \alpha \leq 1 \tag{20}$$

$$\varphi = (1 - \beta)\varphi_{\mathrm{II}} + \beta\varphi_{\mathrm{III}} \qquad 0 \leq \beta \leq 1 \tag{21}$$

$$\varphi = (1 - \gamma)\varphi_{\mathrm{III}} + \gamma\varphi_{\mathrm{IV}} \qquad 0 \leq \gamma \leq 1 \tag{22}$$

Figure 5 shows the auxiliary function $F(K)$, parametrically defined by the last two Eqs. (18):

- for the velocity profiles (20), (21), and (22)
- for the velocity profiles (19)
- for the exact velocity profiles, according to Eq. (1)

Providing we choose the special value of α giving $F = 0$, as Pohlhausen did with Λ, Eq. (20) could improve the description of the stagnation point. But in the field of accelerated flows, Eqs. (20), (21) in two steps, do not improve significantly the results obtained by Pohlhausen in one step only.

A very significant improvement is given instead by Eq. (22) describing the retarded flows, included between points III and IV. The maximum velocity and separation profiles, linearly combined in Eq. (22), are worth further attention.

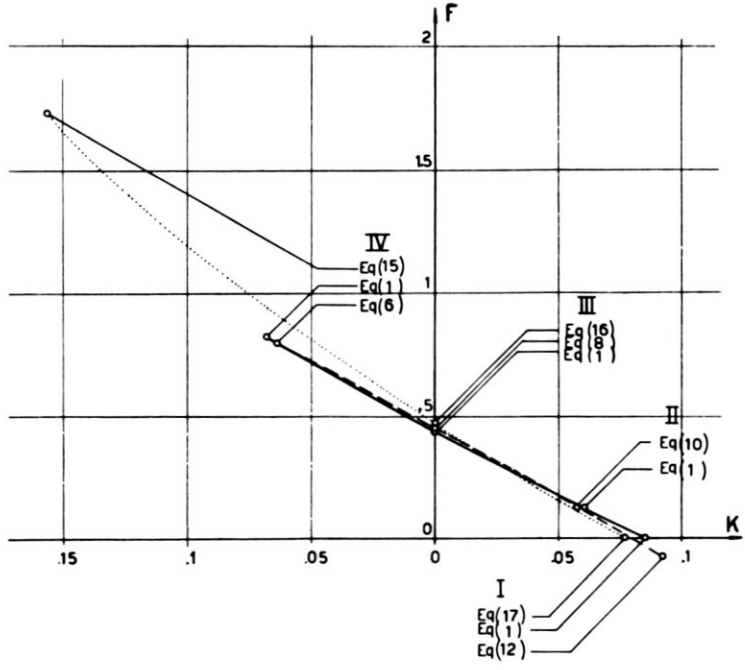

Fig. 5. Auxiliary function $F(K)$ according to: . . . . . Pohlhausen method; – – – present method; —— exact solution of Eq. (1); I, stagnation point; II, τ_0-max point; III, U-max point; IV, separation point.

Profile (6) of separation, only binomial and symmetrical, already proved far better than profile (15) even though trinomial but not symmetrical (Fig. 4).

Profile (8) of maximum velocity, trinomial and antisymmetrical, already proved better than profile (16) also trinomial but not antisymmetrical (Fig. 3).

Such observations emphasize the significance of symmetry and antisymmetry in the boundary layer flows. An interesting framework for all the shear flows can now be given just on the basis of symmetry and antisymmetry.

The boundary-layer flow is guided to inner side by the rigid wall, while it is free at outer side. Hence the boundary-layer flow is half-guided or half-free and must exhibit an intermediate behavior between guided and free flows, which we shall analyze now.

Poiseuille flow is the symmetrical guided flow, having:

$$t = \eta, \qquad \varphi = \eta^2 \tag{23}$$

when seen from an axial observer.

Couette flow is the antisymmetrical guided flow, having:

$$t = 1, \qquad \varphi = \eta \tag{24}$$

when seen from an axial observer.

Wake flow is the symmetrical free flow, having:

$$t = \eta e^{-\eta^2}, \qquad \varphi = 1 - e^{-\eta^2} \tag{25}$$

Mixing flow is the antisymmetrical flow, having:

$$t = e^{-\eta^2}, \qquad \varphi = \operatorname{erf} \eta \tag{26}$$

Table II summarizes t and φ profiles:

- of guided flows (23) and (24) in the first column,
- of half-guided flows (5), (6) and (7), (8) in the second column,
- of free flows (25) and (26) in the third column.

TABLE II

	Guided Flows		Half-guided Flows		Free Flows		
t	Poiseuille	η	Separation	$\eta(1-\eta^2)$	Wake	$\eta e^{-\eta^2}$	Symmetrical Flows
φ		η^2		$2\eta^2 - \eta^4$		$1 - e^{-\eta^2}$	
δ^*/θ		5.000		4.200		3.414	
$\tau_0\theta/\mu U$		0		0		0	
K		−0.0356		−0.0645		−0.1350	
F		0.498		0.800		1.459	
t	Couette	1	Flat Plate	$(1-\eta^2)^2$	Mixing	$e^{-\eta^2}$	Anti-symmetrical Flows
φ		η		$(15\eta - 10\eta^3 + 3\eta^5)/8$		erf η	
δ^*/θ		3.000		2.596		2.414	
$\tau_0\theta/\mu U$		0.167		0.226		0.264	
K		0		0		0	
F		0.334		0.452		0.528	

The first row of Table II describes the symmetrical flows while the second row describes the antisymmetrical flows.

t-profiles of the first row can be obtained from the corresponding ones of the second row:

- through multiplication by η in the first column
- through normalized derivation in the second column
- either through multiplication by η or through normalized derivation in the third column

Figure 6 shows the six velocity profiles of Table II; each profile is drawn with its own scale in order to evidence:

- on the one hand the identical axial behavior of all symmetrical flows and, separately, of all antisymmetrical flows
- on the other hand, the different outer behavior of guided, half-guided and free flows

The numerical values of the shape-factors given by Eqs. (18), calculated and reported in Table II as well, definitely demonstrate that the boundary-layer flows not only qualitatively but also quantitatively place themselves between guided and free flows.

Beside the horizontal and vertical classification on Table II, a diagonal classification is interesting too: white squares include stable laminar flows while hachured squares include unstable laminar flows having inflected velocity profiles.

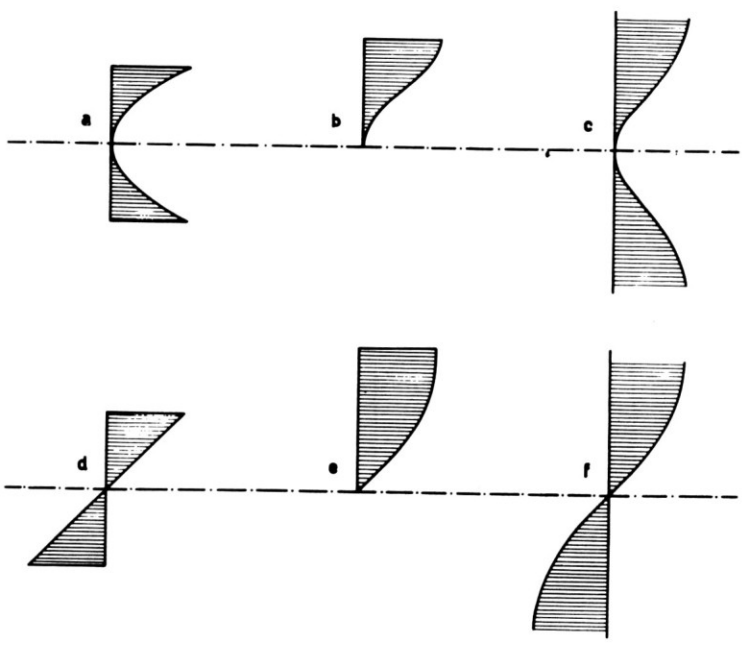

Fig. 6. Laminar velocity profiles for symmetrical and antisymmetrical, guided, half-guided, and free flows: (*a*) Poiseuille flow; (*b*) separating boundary layer; (*c*) wake flow; (*d*) Couette flow; (*e*) flat-plate boundary layer; (*f*) mixing flow.

The rule of progressive derivatives substantially succeeded in improving the picture of the laminar separating flow, that is unfortunately of a typical unstable flow.

But the framework given in Table II allows to pass from the laminar flows to the more interesting turbulent flows.

Figure 7 shows the shear-stress profiles for the six typical flows reported in Table II, and corresponding to the laminar velocity profiles of Fig. 6.

We will show now that such shear-stress profiles are equally shaped for both laminar and turbulent flows, providing τ (or t) is the sum (or the normalized sum) of viscous and Reynolds stresses.

Let us consider, first, the simplest case of guided flows.

Regardless of flow régime, the momentum equation:

- for Poiseuille flow is $\tau_y = p_x$, which implies $\tau \sim y$ or $t = \eta$
- for Couette flow is $\tau_y = 0$, which implies constant τ or $t = 1$

Let us now consider the half-guided flows; here the momentum equation is useless since a priori unknown inertia forces are involved; a direct experimental verification is needed.

As for the separation point Fig. 8 shows the comparison between:

- the exact analytical laminar t-profile according to Hartree (and already given in Fig. 2),
- the experimental turbulent profile, as found by Schubauer and Klebanoff.[3]

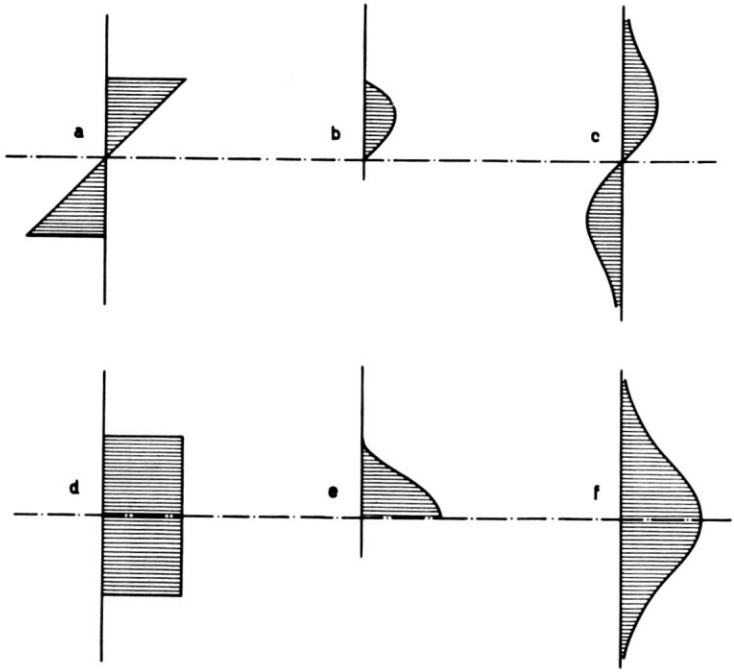

Fig. 7. Laminar and turbulent shear-stress profiles for symmetrical and antisymmetrical, guided, half-guided, and free flows: (*a*) Poiseuille flow; (*b*) separating boundary layer; (*c*) wake flow; (*d*) Couette flow; (*e*) flat-plate boundary layer; (*f*) mixing flow.

Since only the shapes are to be compared, the same maximum and the same slope at the wall were assumed; the agreement is satisfactory.

As for the maximum velocity point (or a flat plate flow), Fig. 9 shows the comparison between:

- the exact analytical laminar t-profile, according to Blasius (and already given in Fig. 2),
- the experimental turbulent profile, as found by Klebanoff.[4]

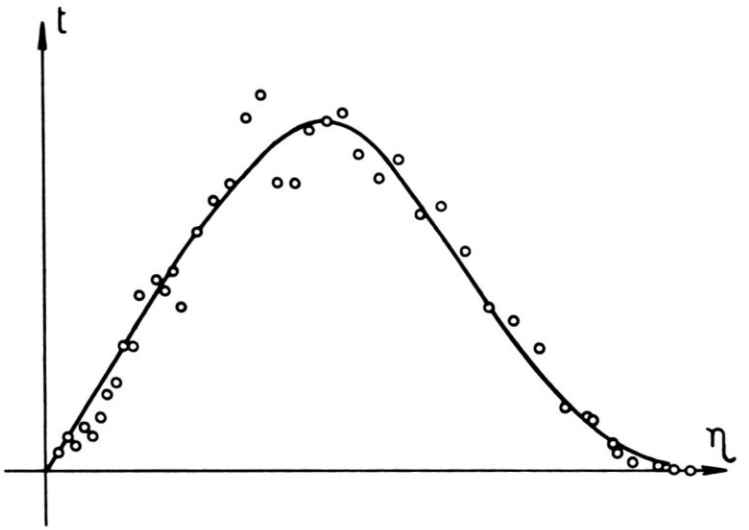

Fig. 8. Comparison between the shear-stress profiles at the separation point, according to: —— analytical solution for the laminar flow; o o o experimental turbulent flow (Schubauer and Klebanoff).

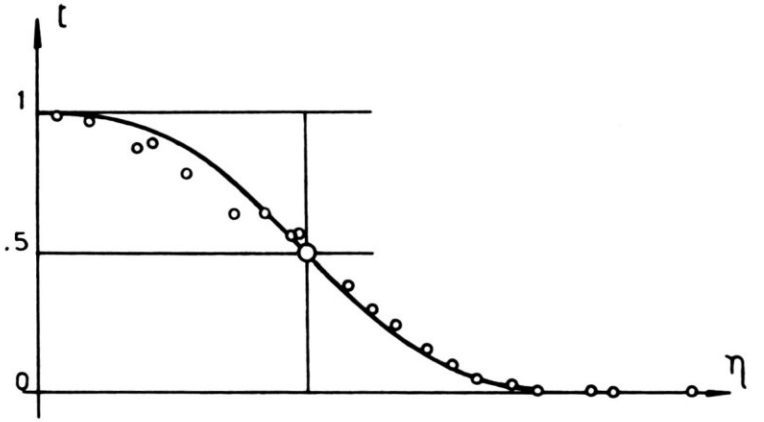

Fig. 9. Comparison between the shear-stress profiles at the point of maximum velocity (or on a flat plate), according to: —— analytical solution for the laminar flow; o o o experimental turbulent flow (Klebanoff).

Since only the shapes are to be compared, the same maximum at the wall and the same width of half stress were assumed; the agreement is again satisfactory.

Let us consider, at last, the free flows. Before analyzing the shear-stress profiles it is to be underlined that the gaussian velocity profiles:

$$\left.\begin{aligned} \varphi &= 1 - e^{-\eta^2} \qquad \text{for wake flow} \\ \varphi &= \operatorname{erf} \eta \qquad \text{for mixing flow} \end{aligned}\right\} \tag{27}$$

given in the third column of Table II, are exactly the turbulent ones experimentally found by Reichardt[1] who took profiles (27) as the basis of his inductive theory of free turbulent flows.

In order to deduce that here, too, the shear-stress profiles are equally shaped for both laminar and turbulent flows, a little qualitative hypothesis is required; namely:

- the eddy viscosity has to be independent from y as, of course, the kinematic viscosity is.

Then the equality of velocity profiles, and hence of their first derivatives, immediately brings about the equality of the transversal shear-stress profiles.

In order to evidence the equality of t-profiles for both laminar and turbulent flows, we had to apply the following hypothesis, at least for the free turbulent flows:

$$\tau = \rho \epsilon u_y \qquad \text{with} \qquad \partial \epsilon / \partial_y = 0 \tag{28}$$

Such hypothesis, even completed with the here unnecessary analysis about physical factors affecting ϵ, was first formulated by Prandtl[1] for the free turbulent flows only; it was extended by Ferrari[5] and Clauser[6] to the outer region of the turbulent boundary layer; it was directly justified by Ferrari[7] and extended to all regions of free turbulence far from rigid walls.

The following two well established hypotheses:

- the total shear-stress profiles are equally shaped for both laminar and turbulent flows

$$t_{\text{lam}} = t_{\text{turb}} \tag{29}$$

- the eddy viscosity is not y-dependent in the regions far from rigid walls

$$\partial \epsilon / \partial y = 0 \tag{30}$$

finally and easily allow to characterize the turbulent velocity profiles as well.

Let us start with free turbulent flows. As already stated, the velocity profiles are the same everywhere for both laminar and turbulent flows. It is noteworthy that the gaussian profiles (27) only represent the linearized analytical solutions for the laminar wake (plane or circular) and for the mixing flow.

As for jets, the analytical exact solutions given by Schlichting[1] for the laminar flow would give different profiles for plane and circular jet, both still different

from gaussian profiles. This difference between analytical laminar jets and experimental turbulent jets shall be explained by keeping in mind that the boundary-layer theory is inadequate in the outer region, far from the axis, where $v \gg u$.

Therefore the experimental evidence that gaussian profiles hold true for all free turbulent flows, shall rather be taken as a proof that the profiles are gaussian even in the laminar field, where experimental evidence cannot be reached because of the well known instability.

Concluding the discussion about free turbulent flows we may state that φ-profiles are again related to laminar or turbulent t-profiles through Eq. (3):

$$\frac{u}{\mu(\infty)} = \frac{\int_0^\eta t \, d\eta}{\int_0^\infty + t \, d\eta} \tag{31}$$

since hypothesis (30) holds true everywhere, lacking rigid walls; in Eq. (31) u is the velocity measured by an axial observer.

As for the turbulent half-guided flows, the two hypotheses (29), (30) bring immediately about that only far from the wall the velocity profiles are equally shaped for both laminar and turbulent flows, namely:

- the turbulent velocity profile approaching the separation is again a laminar separating profile, even though it slips on the wall as was experimentally proved by Schubauer and Klebanoff[3]
- the turbulent velocity profile at the point of maximum velocity (or on a flat plate) is again a Blasius laminar profile, even though it slips on the wall as was stated by Clauser[6] or by Ferrari[7] apart from small corrections.

Concluding the discussion about the half-guided turbulent flows we may state that φ-profiles are again related to laminar or turbulent t-profiles through a modified form of Eq. (3):

$$\frac{u - u^+(0)}{u(1) - u^+(0)} = \frac{\int_0^\eta t \, d\eta}{\int_0^1 t \, d\eta} \tag{32}$$

since hypothesis (30) only holds true far from the wall ($\eta > 0$); in Eq. (32) u is the velocity measured by a wall observer and $u^+(0)$ symbolizes the equivalent slip on the wall, actually described by the universal logarithmic law.

As for turbulent guided flows, the two hypotheses (29), (30) bring immediately about that only far from the two walls the velocity profiles are equally shaped for both laminar and turbulent flows, namely:

- the axial core of a channel or pipe flow is again described by the laminar Poisueille parabola, even though it slips on the walls as was stated by Ferrari[7]
- the axial core of a Couette flow is again described by the laminar Couette straight line, even though it slips on the walls as was experimentally proved by Reichardt[8]

Concluding the discussion about the guided turbulent flows we may state that φ-profiles are again related to laminar or turbulent t-profiles through a modified form of Eq. (3):

$$\frac{u}{u(1) - u^{+}(1)} = \frac{\int_0^{\eta} t \, d\eta}{\int_0^{1} t \, d\eta} \tag{33}$$

since hypothesis (30) only holds true far from the walls ($-1 < \eta < +1$); in Eq. (33) u is the velocity measured by an axial observer and $u^{+}(1)$ symbolizes the equivalent slip on the wall, actually described again by the universal logarithmic law.

To conclude in one sentence the discussion about all the turbulent flows, we state: according to an effective picture given by Clauser for turbulent boundary layers, all the turbulent velocity profiles of guided, half-guided and free flows behave like higher-viscosity laminar profiles; but they slip on a lower-viscosity layer close to the wall, if there is one.

REFERENCES

1. Schlichting, H., *Boundary Layer Theory*, London, Pergamon Press; Karlsrhue, Verlag G. Braun, 1955.
2. Hartree, D. R., "On an Equation Occurring in Falkner and Skan's Approximate Treatment of the Equation of the Boundary Layer," *Proc. Cambridge Phil. Soc.*, vol. 33, part II, 223, 1937.
3. Schubauer, G. B., and P. S. Klebanoff, "Investigation of Separation of the Turbulent Boundary Layer," *NACA TN 2133*, 1950.
4. Klebanoff, P. S., "Characteristics of Turbulence in a Boundary Layer with Zero Pressure Gradient, *NACA TN 3178*, 1954.
5. Ferrari, C., "The Turbulent Boundary Layer in a Compressible Fluid with Positive Pressure Gradient," *J. Aernaut. Sci.*, vol. 18, no. 7, 1951.
6. Clauser, F. H., "The Turbulent Boundary Layer," *Advances in Applied Mechanics*, New York, Academic Press, vol. IV, 1956.
7. Ferrari, C., "Turbolenza di parete (Corso sulla teoria della turbolenza)," *CIME Varenna*, Libr. Ed. Levrotto e Bella, Torino, 1957.
8. Reichardt, H., "Gesetzmässigkeiten der geradlinigen turbulenten Couetteströmung," *Mitt. Max Planck Inst.*, no. 22, Göttingen, 1959.